Chemical Geology 283 (2011) 287–296

Contents lists available at ScienceDirect

Chemical Geology

journal homepage: www.elsevier.com/locate/chemgeo

Research paper

Neon identifies two billion year old fluid component in Kaapvaal Craton

Johanna Lippmann-Pipke [a,*], Barbara Sherwood Lollar [b], Samuel Niedermann [c], Nicole A. Stroncik [c], Rudolf Naumann [c], Esta van Heerden [d], Tullis C. Onstott [e]

[a] Helmholtz Zentrum Dresden Rossendorf, Institute of Radiochemistry, Research Site Leipzig, Permoserstr. 15, 04318 Leipzig, Germany
[b] Department of Geology, University of Toronto, 22 Russell Street, Toronto, Canada M5S 3B1
[c] Helmholtz-Zentrum Potsdam, Deutsches GeoForschungsZentrum, Telegrafenberg, 14473 Potsdam, Germany
[d] Department of Microbial, Biochemical and Food Biotechnology, University of the Free State, P.O. Box 339, Bloemfontein 9300, South Africa
[e] Department of Geosciences, Princeton University, Guyot Hall, Princeton, NJ 08544, USA

ARTICLE INFO

Article history:
Received 20 September 2010
Received in revised form 31 January 2011
Accepted 31 January 2011
Available online 26 February 2011

Editor: J.D. Blum

Keywords:
Noble gas
Neon
Methanogens
Crustal fluid
Metamorphic fluids
Subsurface microbiology

ABSTRACT

The deep gold mines of the Witwatersrand Basin, South Africa have gained recent attention not only because of investigations of the deep fracture water and associated CH_4- and H_2-rich gases found there, but because of recent reports of deep microbial communities persisting to depths of almost 3 km — an exotic outpost of the Earth's deep biosphere. While shallower fluids in the basin (to approximately 1 km) were found to contain abundant populations of methanogens and sulphate-reducing bacteria, the deepest, oldest, most saline fracture waters in the basin hosted hitherto unrecognised low biomass and low biodiversity chemoautotrophic ecosystems independent from the photosphere. Shallow and deep fluids also show distinct differences in gas and fluid geochemistry. Paleometeoric waters are dominated by hydrocarbon gases with compositional and isotopic characteristics consistent with production by methanogens utilising the CO_2 reduction pathway. In contrast the deepest, most saline fracture waters contain gases that are dominated by high concentrations of H_2 gas, and CH_4 and higher hydrocarbon gases with isotopic signatures attributed to abiogenic processes of water–rock reaction. The high salinities (up to hundreds of g/L), highly altered $\delta^{18}O$ and $\delta^{2}H$ signatures, and both ^{36}Cl and measurements of co-occurring nucleogenic noble gases for these fracture waters are consistent with extensive water–rock interaction over geologically long time scales in these high rock/water ratio environments. While the ultimate origin of these fluids has been attributed alternately to saline waters that penetrated the crystalline basement, formation water, or hydrothermal fluids in some cases, their $\delta^{18}O$ and $\delta^{2}H$ isotopic signatures have typically been so profoundly overprinted by the effects of long-term water–rock interaction that, for the most saline end-members, little evidence of their primary composition remains. The key objective of the present study is to further investigate the origin of these fluids by integrating for the first time detailed neon isotope analyses on the dissolved gases. Helium isotopic analysis confirmed that there is no significant mantle-derived component associated with these fluids and gases. Neon isotope results show distinct differences in neon composition that correspond to the different fluid geochemical end-members previously identified. Typical crustal neon signatures (type A) are identified in the paleometeoric waters populated with abundant methanogens. In contrast, the deep more saline fracture waters contain an enriched nucleogenic neon signature unlike any previously reported in crustal fluids. These samples show the highest $^{21}Ne/^{22}Ne$ ratios (0.160 ± 0.003) ever reported in groundwater. Fluid inclusions in these rocks yield even higher $^{21}Ne/^{22}Ne$ ratios between 0.219 and 0.515, consistent with an extrapolated $^{21}Ne/^{22}Ne$ value of 3.3 ± 0.2 at $^{20}Ne/^{22}Ne = 0$. We show that this enriched nucleogenic neon end-member represents a fluid component that was produced in the fluorine-depleted Archaean formations and trapped in fluid inclusions ≥ 2 Ga ago. The observation of enriched nucleogenic neon signatures in deep fracture water implies the release of this billion year old neon component from the fluid inclusions and its accumulation in exceptionally isolated fracture water systems. The observed association of this Archean neon signature with H_2-hydrocarbon-rich geogases of proposed abiogenic origin dissolved in the same deep groundwater suggests that the fracture systems have also allowed for the accumulation of various products of water–rock reactions throughout geologic times. One of these fracture systems contained the deepest characterised microbial ecosystems on earth — chemolithotrophs eking out an existence at maintenance levels independent from sunlight. Consequently, the enriched nucleogenic neon isotope signature may indicate regions in the Archaean crust where investigations of the deep biosphere might be focused.

* Corresponding author. Tel.: +49 341 235 2455; fax: +49 341 235 2731.
E-mail addresses: j.lippmann-pipke@hzdr.de (J. Lippmann-Pipke), bslollar@chem.utoronto.ca (B. Sherwood Lollar), nied@gfz-potsdam.de (S. Niedermann), nicole@gfz-potsdam.de (N.A. Stroncik), rudolf@gfz-potsdam.de (R. Naumann), vheerde@ufs.ac.za (E. van Heerden), tullis@princeton.edu (T.C. Onstott).

0009-2541/$ – see front matter © 2011 Elsevier B.V. All rights reserved.
doi:10.1016/j.chemgeo.2011.01.028

1. Introduction

Noble gas isotope geochemistry has many terrestrial and extraterrestrial applications (Porcelli et al., 2002). The power of these tracers arises from their systematic variation in physical characteristics with mass (e.g., diffusivity and solubility) and lack of chemical reactivity. They have demonstrated their value as inert tracers for characterising subsurface processes, identifying sources and quantifying mass fluxes, because only physical processes modify their abundances (e.g. melting and vapour-phase transport) and numerous radioactive decay schemes produce characteristic changes in their isotopic compositions. A recent progress article highlights the benefits from coupling noble gas studies with carbon geochemistry and carbon isotopic signatures (Sherwood Lollar and Ballentine, 2009). While the inert character of the noble gases provides information on fluid origin, fluid transport and groundwater residence time, carbon geochemistry and isotopic signatures record the history of inorganic and organic reactions that control carbon mobility in fluids in the geosphere and biosphere.

In prior investigations of fracture waters and dissolved gases encountered in the deep gold mines of the Witwatersrand Basin, South Africa, a suite of noble gas isotopes ^{3,4}He, ^{20}Ne, ^{36,38,40}Ar, ^{84}Kr, and ^{132,134,136}Xe established the crustal-radiogenic origin of these fluids (e.g. $^{3}He/^{4}He \sim 10^{-8}$) and provided minimum subsurface residence times for the water ("minimum bulk age") ranging from 1.5 to 23 Ma (Lippmann et al., 2003). This evidence that the most ancient fracture fluids in the basin were effectively isolated from the surface biosphere for millions of years was an important aspect of the microbiological investigations being jointly carried out on these systems. While the shallower fluids in the basin were found to contain abundant populations of methanogens and sulphate-reducing bacteria (Gihring et al., 2006; Moser et al., 2003; Ward et al., 2004), studies showed that the deepest waters in the basin hosted hitherto unrecognised low biomass and low biodiversity chemoautotrophic ecosystems independent from the photosphere and eking out an existence at maintenance levels far from the surface (Chivian et al., 2008; Lin et al., 2006). Isolated systems that trap or isolate organisms over geological time scales may provide new insights into the history and diversity of life on Earth, and are the focus of significant research activity in ice sheets (Karl et al., 1999; Priscu et al., 1999), amber (Cano and Borucki, 1995), rock salt (Vreeland et al., 2000), subseafloor sediments (Parkes et al., 1994) and the deep continental crust (Kerr, 2002; Pedersen, 1997), as well as in the deep fracture waters of the Witwatersrand Basin.

In these prior investigations of the deep fracture water of the Witwatersrand Basin, in addition to noble gas studies (Lippmann et al., 2003), complementary geochemical and stable isotope data on H_2O and on dissolved inorganic carbon (DIC), H_2, CH_4 and higher hydrocarbons were carried out (Lin et al., 2006; Sherwood Lollar et al., 2006, 2008; Ward et al., 2004). Results showed that the fracture waters of the Witwatersrand Basin were comprised of mixtures of two distinctly different groundwater types. At shallower depths, less saline palaeo-meteoric waters with $\delta^{18}O$ and $\delta^{2}H$ signatures falling along the Global Meteoric Water Line (GMWL) contain dissolved hydrocarbons of predominantly microbial origin, and negligible dissolved H_2 gas (Ward et al., 2004). In contrast, deeper fluids typically have a non-meteoric water isotopic signature, high salinity, and high levels of dissolved H_2 (up to 7.5 mmol/l); (Sherwood Lollar et al., 2007) in addition to dissolved hydrocarbons gases (methane, ethane, propane, butane). Based on a variety of lines of geochemical and isotopic evidence, these hydrocarbons are suggested to be produced via abiogenic water–rock reactions, with little or no resolvable contribution from microbial methanogenesis (Sherwood Lollar et al., 2006, 2007; Ward et al., 2004).

In this study, a new sample suite of deep fracture waters from the same sites (Fig. 1a), as well as of fluid inclusions in bulk rock (1b), and vein quartz (1c) from the Witwatersrand Basin were analysed for their Ne isotope composition ($^{20, 21, 22}$Ne). Neon isotopic investigations on

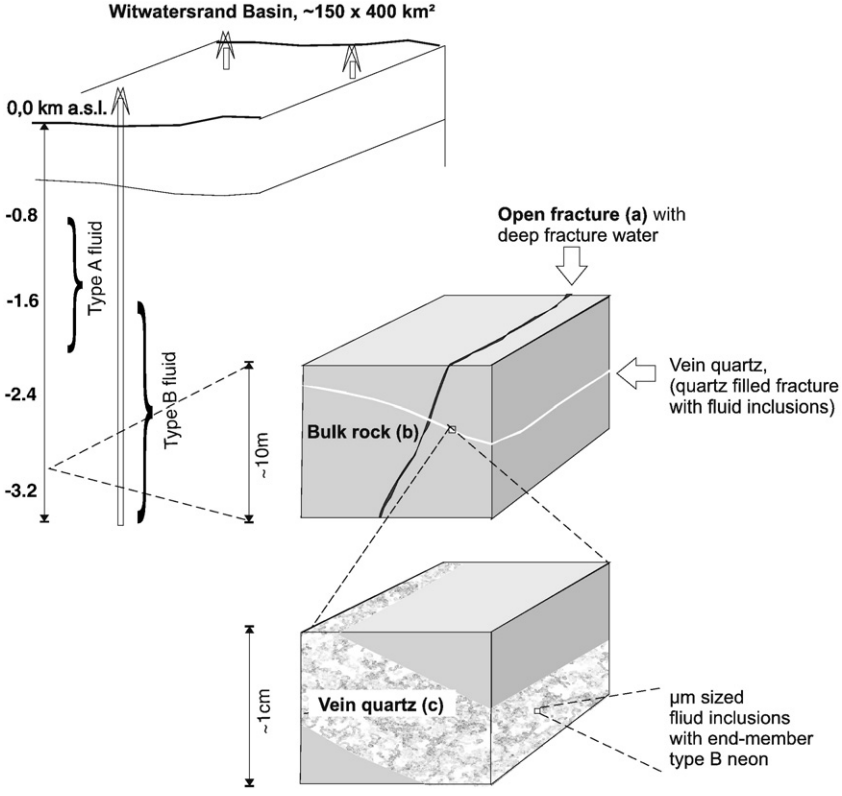

Fig. 1. Schematic of fluid reservoirs under investigation. Three types of samples were collected between 0.8 and 3.3 km depth throughout of the Witwatersrand basin, South Africa. Noble gas concentrations and isotope ratios were determined for a) fracture water samples; b) fluid inclusions in quartzite bulk rock; and c) vein quartz. For a description of different fluid types (A and B, respectively) see Section 4.

fluid samples have proven their particular strength in the quantification of primordial or mantle contributions (Ballentine, 1997; Ballentine and O'Nions, 1991), and for palaeoclimate reconstructions and groundwater dating (Peeters et al., 2002). The objective of this study was to characterise the Ne isotopic composition of the two distinct types of fracture water fluids (paleo-meteoric and deep saline fracture waters) in order to constrain the origin of neon in these different reservoirs; to investigate relationships between the noble gas geochemistry and the reactive gases (H_2, hydrocarbons); and to examine the relationship of fluid geochemistry to the nature and distribution of microbes in the deep subsurface of the Witwatersrand Basin.

2. Geology of the Witwatersrand Basin

The Witwatersrand Basin is well known for its gold mineralization and has thus been intensively investigated. The basin lies within the Archaean Kaapvaal Craton of South Africa and formed episodically between about 3074 Ma and 2714 Ma (Robb and Meyer, 1995) as a result of several discrete tectonomagmatic events (de Wit et al., 1992). The basin is 320 km along a northeasterly axis by 160 km along a northwesterly strike. The Witwatersrand Supergroup is comprised of approximately 7000 m of terrigenous sediment. The Vredefort Dome, near the centre of the basin, formed as the result of a meteorite impact 2025 My ago (Grieve et al., 1990; Leroux et al., 1994; Whiteside et al., 1986). The Witwatersrand Supergroup is underlain by either the 3450 Ma granite–greenstone terrain or by the 3074 Ma volcano-sedimentary Dominion Group and is overlain by the volcanics of the Ventersdorp Supergroup (2714 Ma). The combined sequence of the Dominion, the Witwatersrand and the Ventersdorp strata is also called the Witwatersrand Triad. The Triad is partially covered by the sediments and volcanics of the Transvaal Supergroup (2560 Ma). The southern and eastern portions of the Witwatersrand basin are overlain by the Karoo System (254 to 190 Ma).

The gold and uranium mineralization (locally referred to as the carbon leader) in the Witwatersrand Basin is located within the Central Rand Group, a subgroup of the Witwatersrand Supergroup, and in the Ventersdorp Contact Reef (VCR) which is located at the unconformity between the Witwatersrand and the overlying Ventersdorp Supergroup. The rock formations of the Witwatersrand Supergroup are mostly quartzites and conglomerates and were deposited sometime after 2914 Ma and before 2714 Ma (Armstrong et al., 1991; Robb et al., 1997). The overlying Ventersdorp Supergroup are mostly andesitic lava sequences. The Transvaal sequence consists primarily of a thick dolomitic unit, which acts as an aquifer in large areas of the basin, especially where the dolomite was exposed to weathering processes before being buried under the terrigenous sediments of the Transvaal Supergroup.

In this study, water samples and fluid inclusions from nine different mines in the Witwatersrand Basin were analysed. Site locations and detailed cross-sections are previously published (Gihring et al., 2006; Onstott et al., 2006; Ward et al., 2004). Mponeng mine (26°.25.5′S, 27.25′E), TauTona mine (26.24′S, 27°25′E), Kloof mine (26°24′S, 27°36′E) and Driefontein mine (26°24′S, 27°30′E) are located in the northern margin of the basin, about 80 km south-west of Johannesburg, near Carletonville. Evander mines (26°28′S, 29°05′E) are located approximately 120 km east–south-east of Johannesburg at the eastern extension of the Witwatersrand basin. In most of the Evander Goldfield, the Transvaal and upper parts of the Witwatersrand Supergroup (Central Rand Group) have partially been removed by pre-Karoo erosion. Dolomite exists only in the northern part of the Evander Goldfield. The degree of faulting and structural dislocation within the Evander Goldfield is greater than that encountered at the other gold mines (Tweedie, 1986) (Brand, 1986). Beatrix mine (28°15′S, 26°47′E), Joel mine (28°11′S, 26°43′E), Merriespruit mine (28°07′S, 26°51′E) and Masimong mine (27°56′S, 26°45′E) are located about 240 km south-west of Johannesburg at the southern end of the Witwatersrand Basin.

Table 1
Chemical composition, U, Th, F contents and O/F ratios of selected hanging wall and footwall formations.

Supergroup/mine/formation/comment	Classification	SiO_2	TiO_2	Al_2O_3	Fe_2O_3	MnO	MgO	CaO	Na_2O	K_2O	P_2O_5	H_2O	CO_2	S	U	Th	F	O/F-ratio
		wt.%													ppm	ppm	ppm	atomic
Witwatersrand/Kloof/–/carbon leader	Carbon leader	64.4	0.11	1.2	2.82	<d.l.	0.1	0.14	<d.l.	0.23	0.13	2.52	(26.83)	1.65	11,400	701	56	8120
Witwatersrand/Beatrix/Central Rand/Beatrix reef	Conglomerate	90.0	0.12	3.1	2.29	<d.l.	0.10	0.07	<d.l.	0.73	0.04	0.88	0.14	1.70	174	17.6	66	9220
Witwatersrand/Beatrix/Central Rand/Beatrix reef	Conglomerate	88.3	0.16	2.2	4.35	<d.l.	0.19	0.12	<d.l.	0.43	0.04	0.92	0.18	3.19	123	20.8	74	8120
Witwatersrand/Beatrix/Central Rand/Beatrix reef	Conglomerate	83.9	0.29	4.6	4.97	0.01	0.84	0.07	<d.l.	0.77	0.04	1.34	0.08	2.92	135	16.2	79	7550
Witwatersrand/ Beatrix/–/ hanging	Quartzite	89.2	0.12	7.0	0.18	<d.l.	0.06	0.11	0.20	1.43	0.04	1.27	0.05	0.08	2.4	5.7	61	10,200
Witwatersrand/Beatrix/–/–	quartzite	79.0	0.44	15.4	0.22	<d.l.	0.12	0.07	<d.l.	0.86	0.05	2.81	0.06	0.10	8.4	10.9	78	7970
Witwatersrand/ Beatrix/–/–	Quartzite	93.3	0.14	2.2	2.24	<d.l.	0.38	0.06	<d.l.	0.38	0.04	0.94	0.04	0.11	NA	NA	92	6790
Witwatersrand/Evander/Central Rand/hanging	Quartzite	92.4	0.14	4.4	0.21	<d.l.	0.06	0.06	<d.l.	0.33	0.04	1.47	0.04	0.11	NA	NA	48	13,100
Witwatersrand/Beatrix/Central Rand/footwall	Carbonate vein*	<d.l.	0.02	0.3	16.80	4.64	7.28	27.63	<d.l.	<d.l.	0.05	0.63	43.10	<0.001	NA	NA	87	4300
Witwatersrand/Evander/–/–	Shale	46.0	0.69	14.8	7.83	0.21	9.86	5.20	<d.l.	1.17	0.10	6.28	(7.60)	0.14	NA	NA	284	1900
Transvaal/East Driefontein/ Chuniespoort/–	Dolomite	3.1	0.03	0.4	0.83	0.65	16.80	32.33	<d.l.	0.10	0.08	0.65	45.17	0.04	NA	NA	346	1770
Ventersdorp/Mponeng/–/MP104-VQ1, vein quartz	Quartzite	NA	NA	NA	NA	NA	NA	NA	NA	NA	NA	NA	NA	NA	0.05	0.09	NA	NA
Ventersdorp/Mponeng/–/MP104-VQ1, bedrock	Quartzite	NA	NA	NA	NA	NA	NA	NA	NA	NA	NA	NA	NA	NA	0.5	0.5	NA	NA
Ventersdorp/Mponeng/–/MP104-VQ2, vein quartz	Quartzite	NA	NA	NA	NA	NA	NA	NA	NA	NA	NA	NA	NA	NA	0.02	0.01	NA	NA
Ventersdorp/Mponeng/–/MP104-VQ2, bedrock	Quartzite	NA	NA	NA	NA	NA	NA	NA	NA	NA	NA	NA	NA	NA	0.7	0.9	NA	NA

Uncertainties amount to 10% for U and Th, to 5% for the other elements.
<d.l.: below detection limit (0.004% for MnO, 0.1% for SiO_2, Na_2O, 0.01% for K_2O).
NA: not analysed.
Values in brackets are not considered for the calculation of the oxygen concentration (atom percent), because the carbon is identified as organic carbon and was only oxidised during the analysis.
* mostly ankerite.

Table 2
Noble gas concentrations and isotope ratios in fracture water and fluid inclusions.

Sample	Mine/shaft/ level/site	Sampling date	Geology	Depth	^{4}He	^{3}He/^{4}He		^{20}Ne	^{20}Ne/^{22}Ne	^{21}Ne/^{22}Ne	^{40}Ar	^{40}Ar/^{36}Ar	^{38}Ar/^{36}Ar	^{84}Kr	^{132}Xe	^{134}Xe/^{132}Xe	^{136}Xe/^{132}Xe
				km $_{b.s.}$	$[10^{-4}]$	$[10^{-8}]$	R/R$_a$	$[10^{-7}]$			$[10^{-4}]$			$[10^{-8}]$	$[10^{-9}]$		
					cm^3 g^{-1} $_{water}$			cm^3 g^{-1} $_{water}$			cm^3 g^{-1} $_{water}$			cm^3 g^{-1} $_{water}$	cm^3 g^{-1} $_{water}$		
Surface water																	
ASW	Air saturated water, 20 °C, 1013 mbar				$4.5 \cdot 10^{-4}$	139	1	1.67	9.80	0.029	3.1	295	0.1880	4.0	2.6	0.3879	0.3294
Shallow mine water																	
DR4-IPC	Driefontein /4/–/IPC	29.08.02	Transvaal	0.945	1.62 ± 0.06	2.8 ± 0.2	0.020	1.550 ± 0.031	9.842 ± 0.010	0.0291 ± 0.0010	3.20 ± 0.16	309 ± 9	0.1875 ± 0.0004	4.15 ± 0.21	2.46 ± 0.12	0.3877 ± 0.0025	0.3284 ± 0.0030
Deep fissure water, type A																	
BE16-GDW	Beatrix /1/6/GDW	16.03.01	Witwatersrand	0.866	4.95 ± 0.10	5.5 ± 0.6	0.040	0.090 ± 0.010	10.041 ± 0.019	0.0390 ± 0.0010	1.50 ± 0.07	1476 ± 52	0.1883 ± 0.0026	0.698 ± 0.035	0.519 ± 0.026	0.3962 ± 0.0060	0.3392 ± 0.0054
BE224	Beatrix/2/24/ –	20.06.03	Witwatersrand	0.768	9.32 ± 0.19	2.8 ± 0.6	0.020	0.106 ± 0.010	9.503 ± 0.039	0.0461 ± 0.0006	2.15 ± 0.11	1694 ± 46	0.1889 ± 0.0007	0.837 ± 0.042	0.624 ± 0.031	0.3960 ± 0.0042	0.3390 ± 0.0023
JO121	Joel/1/21/–	17.06.04	Witwatersrand	1.211	15.40 ± 0.31	2.9 ± 0.5	0.021	0.112 ± 0.010	9.160 ± 0.037	0.0663 ± 0.0009	4.49 ± 0.22	2753 ± 63	0.1874 ± 0.0031	0.826 ± 0.041	0.528 ± 0.026	0.4011 ± 0.0064	0.3472 ± 0.0042
MM5-1870	Masimong/5/ 1870/–	02.04.03	Witwatersrand	1.880	10.98 ± 0.22	2.7 ± 0.1	0.019	0.106 ± 0.010	9.303 ± 0.031	0.0538 ± 0.0008	2.64 ± 0.13	2060 ± 61	0.187 ± 0.014	0.700 ± 0.035	0.503 ± 0.025	0.3960 ± 0.0047	0.3421 ± 0.0067
MS149-B53	Merriespruit/ 1/49/B53	11.07.03	Witwatersrand	1.998	2.57 ± 0.05	2.4 ± 0.4	0.017	0.075 ± 0.010	8.908 ± 0.034	0.0679 ± 0.0013	4.11 ± 0.21	3334 ± 90	0.1886 ± 0.0036	0.784 ± 0.039	0.564 ± 0.028	0.4026 ± 0.0058	0.3496 ± 0.0029
MS149-Bh1	Merriespruit/ 1/49/Bh1	20.06.03	Witwatersrand	1.998	15.09 ± 0.30	2.5 ± 0.3	0.018	0.090 ± 0.010	8.947 ± 0.032	0.0648 ± 0.0009	2.98 ± 0.15	3140 ± 84	0.1879 ± 0.0036	0.487 ± 0.024	0.328 ± 0.016	0.4042 ± 0.0050	0.3497 ± 0.0043
MS149-TH3	Merriespruit/ 1/49/TH3	08.02.02	Witwatersrand	1.998	12.02 ± 0.24	2.4 ± 0.3	0.017	0.137 ± 0.010	9.219 ± 0.023	0.0555 ± 0.0010	2.74 ± 0.14	2601 ± 77	0.1905 ± 0.0032	0.503 ± 0.025	0.359 ± 0.018	0.4024 ± 0.0050	0.3489 ± 0.0068
MS151	Merriespruit/ 1/51/–	23.07.03	Witwatersrand	2.028	17.87 ± 0.36	2.5 ± 0.6	0.018	0.109 ± 0.010	8.855 ± 0.026	0.0687 ± 0.0010	4.34 ± 0.22	3243 ± 88	0.1882 ± 0.0017	0.693 ± 0.035	0.430 ± 0.021	0.4031 ± 0.0063	0.3506 ± 0.0029
Deep fissure water, type B																	
DR546-Bh1	Driefontein/ 5/46/Bh1	30.10.01	Ventersdorp	3.213	13.62 ± 0.27	1.5 ± 0.2	0.011	0.119 ± 0.010	9.891 ± 0.021	0.0463 ± 0.0010	16.64 ± 0.83	9020 ± 260	0.1887 ± 0.0021	0.583 ± 0.029	0.388 ± 0.019	0.3975 ± 0.0060	0.3398 ± 0.0050
DR938	Driefontein/ 9/38/CH	07.11.02	Ventersdorp	2.712	3.97 ± 0.08	1.4 ± 0.4	0.010	0.203 ± 0.010	9.812 ± 0.010	0.0292 ± 0.0010	5.18 ± 0.26	377 ± 11	0.1867 ± 0.0004	3.56 ± 0.18	2.51 ± 0.13	0.3872 ± 0.0018	0.3280 ± 0.0016
DR938-CH	Driefontein/ 9/ 38/ CH	12.09.02	Ventersdorp	2.712	5.85 ± 0.12	1.4 ± 0.3	0.010	0.861 ± 0.017	9.762 ± 0.031	0.0304 ± 0.0010	2.87 ± 0.14	418 ± 11	0.1892 ± 0.0009	3.31 ± 0.17	2.20 ± 0.11	0.3878 ± 0.0041	0.3290 ± 0.0029
DR938-H2	Driefontein/ 9/38/H2	30.08.01	Ventersdorp	2.712	7.01 ± 0.14	1.3 ± 0.3	0.009	0.132 ± 0.010	9.537 ± 0.040	0.0534 ± 0.0044	2.12 ± 0.11	1633 ± 47	0.1890 ± 0.0035	0.755 ± 0.038	0.640 ± 0.032	0.4020 ± 0.0038	0.3456 ± 0.0043
DR938-H3	Driefontein/ 9/38/H3	11.07.01	Ventersdorp	2.712	5.22 ± 0.10	1.8 ± 0.3	0.013	0.044 ± 0.010	9.861 ± 0.058	0.0706 ± 0.0006	2.29 ± 0.11	2629 ± 76	NA	0.507 ± 0.025	0.496 ± 0.025	0.4009 ± 0.0060	0.3477 ± 0.0040

EV221	Evander/2/21/–	21.05.02	Witwatersrand	1.624	1.85 ± 0.10	3.9 ± 0.5	0.028	0.230 ± 0.010	9.868 ± 0.077	0.0299 ± 0.0010	0.95 ± 0.10	412 ± 12	0.1888 ± 0.0016	0.801 ± 0.040	0.567 ± 0.028	0.3887 ± 0.0033	0.3311 ± 0.0029
EV818-HeB6	Evander/8/18/HeB6	13.12.02	Witwatersrand	1.830	982 ± 20	1.8 ± 0.8	0.013	1.619 ± 0.032	9.30 ± 0.12	0.1160 ± 0.0005	34.5 ± 1.8	4110 ± 120	0.1879 ± 0.0023	2.57 ± 0.13	1.390 ± 0.070	0.4141 ± 0.0052	0.3660 ± 0.0087
EV821	Evander/8/21/–	16.01.01	Witwatersrand	2.017	3.93 ± 0.08	1.4 ± 0.2	0.010	0.057 ± 0.010	9.126 ± 0.010	0.1593 ± 0.0029	0.99 ± 0.10	3270 ± 100	0.1909 ± 0.0032	0.200 ± 0.010	0.151 ± 0.008	0.4104 ± 0.0071	0.3591 ± 0.0079
KL441-HWDS	Kloof/4/41/HWDS	14.11.01	Witwatersrand	3.300	40.43 ± 0.81	1.3 ± 0.3	0.009	1.327 ± 0.027	9.804 ± 0.018	0.0648 ± 0.0006	16.31 ± 0.82	621 ± 18	0.1875 ± 0.0005	3.47 ± 0.17	2.16 ± 0.11	0.3873 ± 0.0021	0.3280 ± 0.0021
KL739	Kloof/7/39/–	19.08.03	Witwatersrand	3.100	14.24 ± 0.28	1.1 ± 0.2	0.008	0.045 ± 0.010	8.962 ± 0.061	0.1469 ± 0.0016	4.54 ± 0.23	9670 ± 270	0.1869 ± 0.0042	0.309 ± 0.015	0.307 ± 0.015	0.4968 ± 0.0059	0.4744 ± 0.0040
MP104-0	Mponeng/–/104/E65	11.09.02	Ventersdorp	2.825	8.16 ± 0.16	1.5 ± 0.5	0.011	0.231 ± 0.010	9.834 ± 0.018	0.0307 ± 0.0010	2.88 ± 0.14	4400 ± 130	0.1883 ± 0.0007	0.550 ± 0.028	0.350 ± 0.017	0.4365 ± 0.0036	0.3977 ± 0.0028
MP104-1	Mponeng/–/104/E65	16.09.02	Ventersdorp	2.825	16.40 ± 0.33	1.3 ± 0.3	0.009	0.068 ± 0.010	9.341 ± 0.022	0.1415 ± 0.0050	3.36 ± 0.17	5900 ± 180	0.1873 ± 0.0015	0.332 ± 0.017	0.129 ± 0.006	0.461 ± 0.012	0.4277 ± 0.0096
MP104-2	Mponeng/–/104/E65	19.09.02	Ventersdorp	2.825	15.28 ± 0.31	1.7 ± 0.3	0.012	0.054 ± 0.010	8.986 ± 0.081	0.1239 ± 0.0035	3.72 ± 0.19	5680 ± 170	0.1828 ± 0.0037	0.367 ± 0.018	0.298 ± 0.015	0.4643 ± 0.0061	0.4420 ± 0.0054
MP104-3	Mponeng/–/104/E65	27.09.02	Ventersdorp	2.825	25.45 ± 0.51	1.4 ± 0.2	0.010	0.103 ± 0.010	9.293 ± 0.023	0.1209 ± 0.0048	5.95 ± 0.30	5340 ± 150	NA	0.620 ± 0.031	0.493 ± 0.025	0.4573 ± 0.0090	0.4204 ± 0.0075
MP104-4	Mponeng/–/104/–	30.07.04	Ventersdorp	2.825	14.70 ± 0.29	1.0 ± 0.6	0.007	0.049 ± 0.010	9.462 ± 0.032	0.1600 ± 0.0029	3.88 ± 0.19	8320 ± 190	0.1878 ± 0.0026	0.253 ± 0.013	0.253 ± 0.013	0.5534 ± 0.0091	0.554 ± 0.011
					$[10^{-6}]$ $cm^3\ g^{-1}_{rock}$			$[10^{-12}]$ $cm^3\ g^{-1}_{rock}$			$[10^{-8}]$ $cm^3\ g^{-1}_{rock}$			$[10^{-12}]$ $cm^3\ g^{-1}_{rock}$	$[10^{-12}]$ $cm^3\ g^{-1}_{rock}$		
Fluid inclusions, vein quartz																	
MP104-VQ1	Mponeng/–/104/–	16.09.02	Ventersdorp	2.825	67 ± 11	1.5 ± 0.1	0.011	15.3 ± 1.1	8.23 ± 0.28	0.497 ± 0.018	670 ± 82	111,000 ± 67,000	NA	3.24 ± 0.31	1.10 ± 0.25	0.4091 ± 0.0086	0.3519 ± 0.0096
MP104-VQ2	Mponeng/–/104/–	16.09.02	Ventersdorp	2.825	23.6 ± 2.6	1.4 ± 0.3	0.010	17.8 ± 1.4	8.73 ± 0.44	0.585 ± 0.044	940 ± 140	277,000 ± 53,000	0.1837 ± 0.0083	7.66 ± 0.90	3.07 ± 0.51	0.401 ± 0.015	0.3510 ± 0.0081
Weighted mean																	
Fluid inclusions, bulk rock																	
TT118-BR1	Tautona/–/118/–	31.01.06	Witwatersrand	3.540	49.2 ± 4.6	1.1 ± 0.2	0.008	125 ± 17	9.40 ± 0.20	0.219 ± 0.023	420 ± 52	23,300 ± 360	0.1850 ± 0.0035	6.05 ± 0.82	3.37 ± 0.51	0.407 ± 0.033	0.356 ± 0.039
For comparison: fluid inclusions, anorthosite																	
Greenland-S1°	Fiskenaesset Complex				620 ± 60			380 ± 40	3.9 ± 0.4	0.48 ± 0.05							
Greenland-S2°	Fiskenaesset Complex				480 ± 50			390 ± 40	5.4 ± 0.6	0.42 ± 0.07							
Greenland-S3°	Fiskenaesset Complex							630 ± 50	5.7 ± 0.4	0.33 ± 0.04							

NA: not analysed.
° data from Zadnik and Jeffrey (1985).

At the Beatrix mines the Witwatersrand Supergroup lies beneath 400 to 800 m of carboniferous Karoo sediments (Tweedie, 1986).

Major and trace element analysis of selected reefs, hanging wall and footwall formations are shown in Table 1. The Witwatersrand Kloof carbon leader was selected since it is known to be the higher U content end-member in the basin. At the other end of the spectrum, Beatrix reef was selected for its known generally low U content.

3. Methods

Mining-related drilling operations allowed the sampling of water-bearing fractures soon after their intersection, at depths ranging from about 0.8 to 3.3 km below surface. A total of 24 sample suites were collected at the collars of 20 different exploration boreholes in 9 deep gold mines from across the Witwatersrand Basin. The standard sampling procedures for gas and fracture water samples and rigorous approaches for constraining contamination from either sampling activities or mining operations are described elsewhere (Lippmann et al., 2003; Sherwood Lollar et al., 2002; Ward et al., 2004). The noble gas data presented in Table 2 were obtained in the noble gas lab of the GFZ Potsdam, which is equipped with a water degassing line, a mechanical crusher for rock samples, a gas purification line, two cold heads for the cryogenic separation of noble gases and a VG5400 mass spectrometer (Niedermann et al., 1997, 2007; Stroncik et al., 2007).

For the major and trace element analysis (Table 1) and for noble gas analysis of the fluid inclusions (Table 2), rock samples from the Witwatersrand Supergroup were taken at selected water and gas sampling sites. The analysis of the elemental composition by means of XRF and ICP-MS and the mineral composition by XRD, as well as the quantification of F by means of potentiometric measurement after pyrohydrolysis, were performed at the GFZ Potsdam.

The methods and results of compositional analysis of the gas samples from the same boreholes (N_2, H_2, O_2, He, Ar, CH_4, C_2H_6, C_3H_8, and C_4H_{10}), and the isotopic signatures of water and the hydrocarbons were previously published (Sherwood Lollar et al., 2006, 2008, 2007; Ward et al., 2004).

4. Results

In a neon three-isotope plot, a group of fracture water samples (Fig. 2, open diamonds, "type A") are identical to air or plot along the (solid) line between air composition ($^{20}Ne/^{22}Ne = 9.8$, $^{21}Ne/^{22}Ne = 0.029$) and a crustal end-member with an extrapolated $^{21}Ne/^{22}Ne = 0.47$ at $^{20}Ne/^{22}Ne = 0$, consistent with what has been traditionally observed for crustal fluids (Ballentine, 1997; Ballentine and Burnard, 2002; Bottomley et al., 1984; Kennedy et al., 1990). All other fracture water samples (filled diamonds, "type B") fall off this "crustal line" on a much flatter trend, reflecting a large neon anomaly compared to any previous studies of crustal fluids. Their maximum measured $^{21}Ne/^{22}Ne$ ratio of 0.160 ± 0.003 (Table 2) has not been previously reported in any groundwater system. Analysis of neon from fluid inclusions in crushed local bulk rock material (filled circle) from one of the fracture water sites (TauTona) reveals a $^{21}Ne/^{22}Ne$ ratio of 0.219 ± 0.023 plotting on the same trend. Fluid inclusions in crushed vein quartz samples (filled triangles) yield even higher $^{21}Ne/^{22}Ne$ ratios with a weighted mean ratio of 0.515 ± 0.017 (filled triangle with white dot). We know of only one other study on fluid inclusions in anorthosite from Western Greenland (cross symbols) (Azuma et al., 1993; Zadnik and Jeffery, 1985) with comparably high $^{21}Ne/^{22}Ne$ ratios (between 0.33 ± 0.04 and 0.48 ± 0.05, Table 2). They represent a neon signature about midway between the type A and type B patterns described here. Assuming that the fluid inclusions in the crushed vein quartz represent the end-member composition of type B neon, a mixing line can be drawn between air and the weighted mean of these fluid inclusions (dashed line in Fig. 2). This line is characterised by an extrapolated $^{21}Ne/^{22}Ne$ value of 3.3 ± 0.2 at $^{20}Ne/^{22}Ne = 0$.

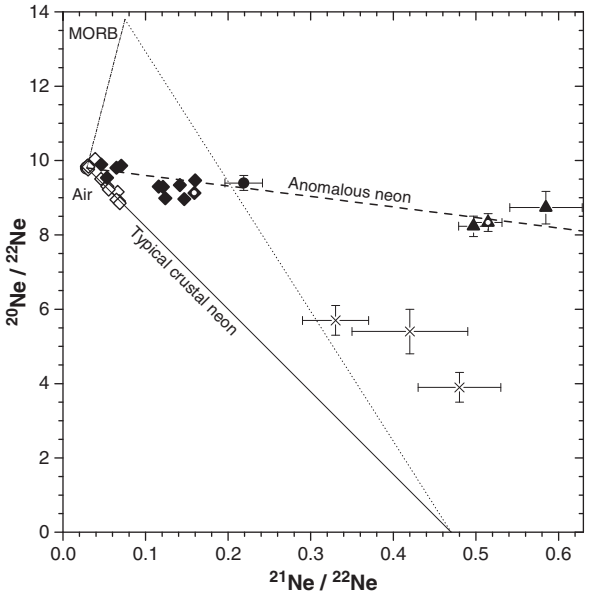

Fig. 2. Neon isotope signatures ($^{20}Ne/^{22}Ne$ versus $^{21}Ne/^{22}Ne$) of fracture waters, fluid inclusions in bulk rock, and fluid inclusions in vein quartz from the Witwatersrand Basin. Fracture water (open and filled diamonds) and fluid inclusions from quartzite bulk rock (filled circle) and from vein quartz (filled triangles) are shown. Fluid inclusion data from an Archaean anorthosite from Western Greenland (Zadnik and Jeffery, 1985) (crosses) are plotted for comparison. Typical crustal fluids (type A, open diamonds) fall along the *solid* mixing line (Kennedy et al., 1990) between Air and $^{21}Ne/^{22}Ne = (0.47–0.79)$ at $^{20}Ne/^{22}Ne = 0$. All fluids with an enriched nucleogenic neon signature (type B, filled symbols — see text Section 4) fall along the *dashed* line that suggests mixing between air-derived neon and a crustal end-member represented by the weighted mean of the fluid inclusions in vein quartz (filled triangle with white dot). A mixing line drawn through these samples is characterised by an extrapolated $^{21}Ne/^{22}Ne$ value of 3.3 ± 0.2 at $^{20}Ne/^{22}Ne = 0$. The type B samples represent the highest ever-measured $^{21}Ne/^{22}Ne$ ratios in ground water or fluid inclusions. The dotted line represent the theoretical line along which samples would fall if there were derived exclusively from a two-component mixing between mantle-derived (MORB) and typical crystal-derived neon.

For two reasons, type B neon cannot simply be due to mixing between type A neon (typical crustal) and a mantle neon component (MORB, Fig. 2), as suggested for fluids sampled in other areas of the world where crustal extension is occurring and indicated by the dotted line in Fig. 2 (Ballentine, 1997). First, the $^3He/^4He$ values of type B samples are $< 4 \cdot 10^{-8}$ (Table 2), indicating a crustal origin and excluding any significant mantle contribution. Second, the observed high $^{21}Ne/^{22}Ne$ ratios in the fluid inclusions do not lie within the mixing triangle between air, mantle (MORB, mid ocean ridge basalt, $^{20}Ne/^{22}Ne \leq 13.8$, $^{21}Ne/^{22}Ne \leq 0.075$) and a crustal source (Fig. 2).

Since these data cannot be attributed to mixing between mantle-derived (MORB), air-derived and typical crustal-derived neon components, the data reveal two striking features. First, two distinctly different nucleogenic neon components are identified — a typical crustal one with $^{21}Ne/^{22}Ne$ end-member values ranging between 0.47 and 0.79 (Ballentine, 1997; Ballentine and Burnard, 2002; Kennedy et al., 1990) (type A) and an enriched nucleogenic, previously unrecognised crustal neon component with an end-member ratio of $^{21}Ne/^{22}Ne = 3.3 \pm 0.2$ (type B). Second, the $^{21}Ne/^{22}Ne$ ratios of the type B fluids are to our knowledge the highest ever measured in groundwater or in fluid inclusions.

5. Discussion

5.1. Origin of the enriched nucleogenic neon component

It has long been established that the production of nucleogenic neon in Mg-poor continental crust is predominantly due to the nuclear reactions $^{17,18}O(\alpha,n)^{20,21}Ne$, $^{19}F(\alpha,n)^{22}Na(\beta^+)^{22}Ne$ and $^{19}F(\alpha,p)^{22}Ne$

(Wetherill, 1954). Hence the production ratio of the nucleogenic neon isotopes, $^{21}Ne/^{22}Ne$, depends on the ratio of the target-elements (O/F) in the ~40 μm reaction range of α particles (Ballentine and Burnard, 2002) around the U and Th nuclei providing them. Indeed, experimental studies performed with U-rich minerals confirmed the expected relationship between their O/F ratio and the $^{21}Ne/^{22}Ne$ production ratio (Hünemohr, 1989). However, in field studies, typical crustal formations showed $^{21}Ne/^{22}Ne$ production ratios about eight times lower than those expected based on the bulk O/F ratio of average crust (Ballentine, 1997; Ballentine and Burnard, 2002; Kennedy et al., 1990). This discrepancy has been interpreted to reflect a preferential association of the α-emitting U and Th with certain common and widely distributed F-bearing crustal minerals, like micas and amphiboles (Kennedy et al., 1990). The O/F ratio in the ~40 μm reaction range of α particles required to generate the typical crustal neon isotopic signatures of $^{21}Ne/^{22}Ne = (0.47–0.79)$ was inferred to be ~110 (atomic), again, significantly lower than the crustal bulk O/F ratio (Hünemohr, 1989) with reference to (Mason and Moore, 1981).

In our study, geochemical analyses of rock samples from the Archaean Witwatersrand Supergroup collected from across the basin yielded ~10 fold greater bulk O/F ratios than typical crustal values, ranging between 6800 and 13,100 (Table 1, quartzites and conglomerates) with a calculated mean and standard deviation of 8100 ± 1100. This anomalous high bulk O/F value – reflecting a substantial depletion in F compared with average continental crust – provides a reasonable source for the enriched nucleogenic $^{21}Ne/^{22}Ne$ production ratio of 3.3 ± 0.2 observed in the type B fluid.

5.2. Preservation of the observed large ^{21}Ne excesses in fluid inclusions

The highest $^{21}Ne/^{22}Ne$ ratios - including the assumed end-member of the type B fluid - are found in fluid inclusions (Fig. 1c; Fig. 2, triangles). Fluid inclusions have the potential to preserve fluids and their geochemical and isotopic signature through geologic time (Azuma et al., 1993; Roedder, 1990; Stuart and Turner, 1992; Turner et al., 1988; Zadnik and Jeffery, 1985). The formation of the fluid inclusions in the vein quartz of the Ventersdorp formation and in the bulk rock is thought to be related to one of the last major regional metamorphic events occurring between 2.7 and 2.0 Ga (Klemd, 1999; Robb et al., 1997). We suggest that the major fraction of the $^{21}Ne_{nucl}$ in the inclusions represents such a metamorphic fluid component trapped during formation of vein quartz ≥2 Ga ago during this last period of regional metamorphism, by demonstrating that other possible sources – specifically ^{21}Ne diffusion from the vein quartz into the fluid inclusions after their formation – has a negligible effect.

This argument is based on the assumptions that initial neon isotope ratio in the fluid inclusions must have been air-like, and that the initial ^{20}Ne concentration was similar to the measured ^{20}Ne concentration (Table 2). We estimate the $^{21}Ne_{nucl}$ in-situ production in vein quartz in since the last regional metamorphic event in the Kaapvaal Craton 2 Ga ago (Robb et al., 1997) on the basis of measured U (0.05 and 0.02 ppm) and Th contents (0.09 and 0.01 ppm), respectively (Table 1, MP104-VQ1 and VQ2, vein quartz). We further consider a $^{21}Ne/^{22}Ne$ production ratio of 3.3 based on extrapolation from the ratios observed in the type B fluid samples (Fig. 2). We assume that the vein quartz is an open system with only a certain retained neon fraction (Λ) of the ^{21}Ne produced therein being retained. As we know of only one study that has explicitly quantified the neon fraction retained in crustal formations since the last metamorphic event (Drescher et al., 1998), we consider their value of $\Lambda = 23\%$ as a rough estimate, with another 5–10% thereof diffusing into the fluid inclusions while the rest is lost to the outside (Drescher et al., 1998). Based on this model, the calculated $^{21}Ne/^{22}Ne$ ratios in the fluid inclusions would range between 0.039 ± 0.007 and 0.032 ± 0.002 for the samples VQ1 and VQ2. Since these calculated values are more than an order of magnitude lower than the measured values of $^{21}Ne/^{22}Ne$ ratios in the fluid inclusions (0.497 ± 0.018 and 0.585 ± 0.044 for MP104-VQ1 and VQ2, respectively) (Table 2), any contribution from post-inclusion process neon diffusion from the vein quartz into the fluid inclusion reservoirs must be negligible. In fact, even if the highly unrealistic scenario of 100% neon retention ($\Lambda = 100\%$) is considered, post-formation diffusion of neon into the fluid inclusions could not explain the observed $^{21}Ne/^{22}Ne$ ratio of sample VQ2. We conclude that the major fraction of the $^{21}Ne_{nucl}$ in the fluid inclusions represents an inherited provenance from metamorphic fluid flow (Klemd et al., 1989) related to one of the last major regional metamorphic periods between 2.7 and 2.0 Ga (Klemd, 1999; Robb et al., 1997) with uptake of the type B neon signature from Archaean fluorine-depleted formations prior to its trapping in fluid inclusions during formation of the quartz veins. Presumably the included radiogenic $^{40}Ar_{rad}$ (Table 2), produced by radioactive decay (electron capture) of ^{40}K, also originates from the metamorphic fluids to a large fraction.

5.3. Accumulation of type B neon in fracture waters

Based on this interpretation of the origin of the enriched nucleogenic neon signature, and its trapping in the fluid inclusions, we now consider the implications of finding this signature in some of the bulk groundwater fluids in the Witwatersrand basin as well as in the fluid inclusions. Mass balance calculations from fluid inclusion studies have demonstrated that fluid inclusion leakage may be a major source of dissolved solutes in hydrogeologically isolated fracture water systems in other Precambrian Shield settings (Nordstrom et al., 1989). The type B fracture water samples could have acquired their enriched nucleogenic neon signal simply by uptake of up to ~30% ^{21}Ne from leaking fluid inclusions.

Alternatively, the calculated time needed to produce the enriched nucleogenic $^{21}Ne/^{22}Ne$ ratio in the bulk rock and to accumulate it in the fracture water (up to the observed ratio of 0.16), along with the observed $^{40}Ar/^{36}Ar$ (up to 9670) and $^{3}He/^{4}He$ signatures ($3.9 \cdot 10^{-8}$), amounts to about 40 Ma. This estimate is based on production in quartzite (Table 1) and subsequent release (1-Λ) into free fluids that are depleted with respect to atmospheric noble gases (Lippmann et al., 2003; Ma et al., 2009) and implies a rock to water mass ratio of 1000, so that the $\sim 3 \cdot 10^{-7}$ cm^3 $^{40}Ar_{rad}$ produced per gram of rock would explain the observed $\sim(1–4) \cdot 10^{-4}$ cm^3 $^{40}Ar_{rad}$ g^{-1}_{water} in the fracture water samples. An influence of the thin, ore-bearing, U-rich layers, present across the Witwatersrand Basin (Johnson et al., 2006; Johnston, 2009) (e.g. the carbon leader reef, ~1.1 wt.% U, <0.2 wt.%K, Table 1) on the type B end-member isotope signature is possible, but unlikely, because its U, Th and K contents could not explain the neon and argon signatures consistently. Due to the high U content the ratio of the production rates of $^{21}Ne_{nucl}$ and $^{40}Ar_{rad}$ in Carbon Leader is five orders of magnitude larger than those that would explain the observed $^{21}Ne/^{40}Ar$ values in the fluid inclusions.

5.4. Relationship of neon components to H_2, hydrocarbons and deep subsurface microbial communities

Previous studies of the compositional and isotopic signatures of other dissolved gases in deep South African fracture water showed that the dominant components are reduced gases including CH_4, H_2 and higher hydrocarbons (Sherwood Lollar et al., 2006; Ward et al., 2004). Within paleometeoric waters in the Witwatersrand basin, methane and other dissolved hydrocarbon gases were found to be predominantly microbial in origin — a conclusion supported by culture-based and molecular microbiological results that identified active populations of methanogens in these less saline waters (Gihring et al., 2006; Onstott et al., 2006; Ward et al., 2004). In deeper, more saline fracture waters however, samples showed elevated levels of dissolved H_2 (up to 7.5 mmol/l (Sherwood Lollar et al., 2007)) and distinct isotopic pattern in the hydrocarbon gases and have been used to argue that these gases are the products of abiogenic water–rock reactions (specifically, H_2 production by radiolysis (Lin et al.,

2005a, 2006, 2005b)) and hydrocarbon production by abiogenic polymerization (Sherwood Lollar et al., 2006, 2008).

A comparison of the previous data with the results of this noble gas study reveals that the enriched nucleogenic neon signature (Fig. 2, filled symbols) is found in the same samples for which high H_2 and proposed abiogenic hydrocarbons have been identified (yellow circles Fig. 3). In these most saline fracture waters at Kloof, Driefontein, Mponeng and TauTona mines at depths of 2.7 to 3.6 km, groundwater temperatures range between 45 °C and >60 °C, and $\delta^{18}O$ and $\delta^{2}H$ values that fall to the far left and above the global meteoric water line (Ward et al., 2004) as is typical of deep groundwater at other Precambrian Shield sites worldwide and consistent with the effects of extensive water–rock reaction over geologically long timescales (Frape and Fritz, 1987; Kloppmann et al., 2002). In contrast, at those sites where typical crustal neon has been identified (type A, open diamonds in Fig. 2 — Beatrix, Masimong, Merriespruit and Joel mines at depths of 0.8 to 2 km), the CH_4 has been shown to be predominantly microbial in origin (green symbols Fig. 3) (Lin et al., 2006; Sherwood Lollar et al., 2006, 2008; Ward et al., 2004). At these sites, low salinity groundwaters with temperatures ranging between 30 and >60 °C have $\delta^{18}O$ and $\delta^{2}H$ signatures that fall along the Global Meteoric Water Line (Craig, 1961), but are depleted in ^{18}O and ^{2}H relative to modern precipitation, indicating a palaeo-meteoric origin (Lippmann et al., 2003; Ward et al., 2004). There is only one partial exception. One type B fracture fluid from Evander mine (depth of 1.6 to 2 km) (EV821, filled diamond with white dot in Fig. 2) was analysed for H_2 and hydrocarbon gas, but hydrocarbon isotopic signatures indicated a mixed origin with both microbial and abiogenic characteristics.

5.5. Implications for earth's habitability and the deep biosphere

The end-member composition of the deep saline fracture water where type B neon occurs is rich in substrates due to abundant H_2, CH_4 and higher hydrocarbons (Lin et al., 2005a, 2006; Sherwood Lollar et al., 2007). Several recent studies have documented the distinctive microbial communities in this deepest component of the planet's biosphere, where chemoautotrophic ecosystems eke out an existence at maintenance levels far from the surface (Chivian et al., 2008; Lin et al., 2006). Characterised by low biodiversity, these SO_4-reducing H_2 autotrophic communities have to date only been successfully identified at a handful of sites in the Witwatersrand Basin, in large part due to their extremely low biomass. The communities described (Chivian et al., 2008; Lin et al., 2006) in fact correspond to the site in this study (Mponeng) where the largest contribution of type B neon has been discovered (Table 2; Fig. 3). Hence the results of this noble gas study suggest that the enriched nucleogenic type B neon signature may serve as a proxy search strategy for identification of regions of the earth's crust where additional investigations of the deep biosphere might be focussed. In the geologic past, the occurrence of such fluids may have been a much more widespread feature than today, but the such H_2-rich reservoirs may in most instances have been depleted over geologic time by releasing their contents, as tectonic shifts triggered the opening of fractures (Sherwood Lollar et al., 2007; Sleep and Zoback, 2007), and by microbial depletion of substrates, and because their distinct isotopic and geochemical signatures got successively overprinted by mixing with younger palaeometeoric waters and with products of biological cycling of carbon by micro-organisms (Sherwood Lollar et al., 2006; Ward et al., 2004). Consequently, occurrences of such ancient fluids identified here by the type B neon signature, high H_2 levels and abiogenic hydrocarbon isotopic signatures have become very rare in the dynamic, inhabited upper crust. Determining the breadth and depth of such occurrences will be significant both in terms of defining the limits of life in the earth's deep crust and for evaluating the proportion of the earth's biomass attributable to the deep biosphere — estimated by some to equal that of the planet's total surface biomass (Whitman et al., 1998).

6. Conclusions

We interpret the relationships between these four independent geochemical systems the isotopic signature of the dissolved neon

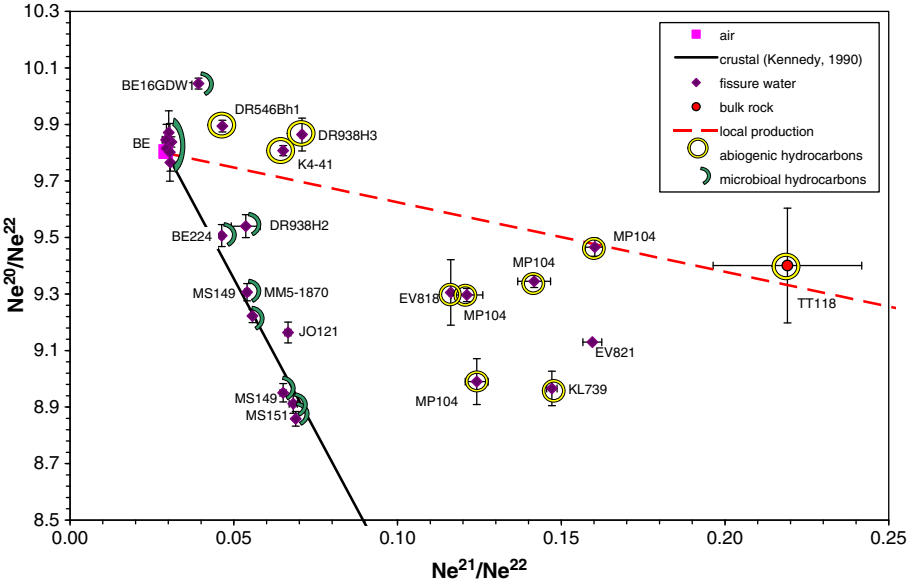

Fig. 3. Neon isotope signatures ($^{20}Ne/^{22}Ne$ versus $^{21}Ne/^{22}Ne$) of fracture waters from the Witwatersrand Basin (expanded scale) Neon isotopic signatures are shown for fracture water samples from each mine site (MP — Mponeng, EV — Evander, KL — Kloof, DR — Driefontein; BE — Beatrix; MS — Masimong; JO — Joel, MM — Merrispruit). One sample from a bulk rock fluid inclusion from TauTona mine (TT) is shown for comparison. The dissolved hydrocarbons of the type A fracture water samples (typical crustal neon) all have isotopic and geochemical signatures that support a microbial origin for the hydrocarbons (samples in green) (Ward et al., 2004). In contrast, at sites where isotopic and geochemical signatures support a proposed abiogenic origin for hydrocarbons (yellow symbols) along with high concentrations of dissolved H_2 (Sherwood Lollar et al., 2006, 2008, 2007; Ward et al., 2004), there is a significant component of the type B samples (enriched nucleogenic neon). Typical crustal fluids fall along the solid mixing line (Kennedy et al., 1990) between air-derived neon and a crustal end-member with an intercept of $^{21}Ne/^{22}Ne = (0.47–0.79)$ at $^{20}Ne/^{22}Ne = 0$. All fluids with an enriched nucleogenic neon signature (type B see Fig. 2) fall along the dashed line that suggests mixing between air-derived neon and a crustal end-member represented by the weighted mean of the fluid inclusions in vein quartz (as per Fig. 2). A mixing line drawn through these samples is characterised by an extrapolated $^{21}Ne/^{22}Ne$ value of 3.3 ± 0.2 at $^{20}Ne/^{22}Ne = 0$.

determined in this study, and previously published results (the isotopic and geochemical signatures of the reactive gases (H_2, CH_4 and the higher hydrocarbons), the stable isotopes of water, and salinity trends) as due to the parallel existence of two distinctly different crustal fluid networks. The fracture systems that host type B fluids are hydrogeologically isolated reservoirs, virtual "time capsules", which over timescales of several Ma progressively accumulate fluids released from a variety of processes. These include the leakage of fluid inclusions (with ≥2 Ga old metamorphic fluids representing the enriched nucleogenic neon end-member) and extensive water rock interactions producing the mmol/l levels of H_2, hydrocarbons of proposed abiogenic origin and dissolved solutes that enhance the salinity (Bottomley et al., 1994; Frape and Fritz, 1987; Kloppmann et al., 2002; Sherwood Lollar et al., 1993, 2006, 2007). Significantly, the bulk of the fracture fluid, the enriched nucleogenic neon isotopic signature and the dissolved H_2 and hydrocarbons are not necessarily all of the same age. We suggest only that the enriched nucleogenic neon in the fluid inclusions is a ≥2 Ga old metamorphic fluid component resulting from production by natural nuclear reactions in F-depleted Archaean formations, with subsequent accumulation in hydrogeologically isolated fracture fluids (with minimum bulk residence time estimates of millions of years) that are characterised by significant quantities of accumulated products of potentially much later water–rock reactions. The enriched nucleogenic type B neon may serve as an independent tracer of the oldest, most saline fracture waters in the basin, which are not influenced by microbial methanogenesis but are rich in H_2 and proposed abiogenic hydrocarbons.

Acknowledgements

We thank the subsurface sampling team members E. Boice, M. Davidson, T. Gihring, B. Gilhooly, J. Hall, T. Kieft, S. Knoesson, L.-H. Lin, D. Litthauer, S. McCuddy, D. Moser, S. Pfiffner, T. Phelps, L. Pratt, T. Prey, C. Ralston, B. Silver, G. Slater, B. Tipple, G. Wanger, and A. Welty for their excellent cooperation, and K. Hahne, H. Rothe, C. Schößler, G. Lacrampe-Couloume and E. Schnabel for technical assistance. This study was supported in parts by grants from the Deutsche Forschungsgemeinschaft (German Science Foundation) and the GFZ Potsdam to J.L.P., the Natural Sciences and Engineering Research Council of Canada and the Canada Research Chairs Program to B.S.L, and by the U.S. National Science Foundation Life in Extreme Environments Program to T.C.O. Thanks are owed to two reviewers (C.J. Ballentine and one anonymous) for their helpful comments and suggestions.

References

Armstrong, R.A., Compston, W., Retief, E.A., Williams, I.S., Welke, H.J., 1991. Zircon ion microprobe studies bearing on the age and evolution of the Witwatersrand triad. Precambrian Res. 53 (3–4), 243–266.

Azuma, S.-I., Ozima, M., Hiyagon, H., 1993. Anomalous neon and xenon in an Archaean anorthosite from West Greenland. Earth Planet. Sci. Lett. 114 (2–3), 341–352.

Ballentine, C.J., 1997. Resolving the mantle He/Ne and crustal $^{21}Ne/^{22}Ne$ in well gases. Earth Planet. Sci. Lett. 152, 233–249.

Ballentine, C.J., Burnard, P.G., 2002. Production, release and transport of noble gases in the continental crust. Rev. Mineral. Geochem. 47, 481–538.

Ballentine, C.J., O'Nions, R.K., 1991. The nature of mantle neon contributions to Vienna Basin hydrocarbon reservoirs. Earth Planet. Sci. Lett. 113, 553–567.

Bottomley, D.J., Ross, J.D., Clarke, W.B., 1984. Helium and neon geochemistry of some groundwaters from the Canadian Precambrian Shield. Geochim. Cosmochim. Acta 48, 1973–1985.

Bottomley, D.J., Gregoire, D.C., Raven, K.G., 1994. Saline ground waters and brines in the Canadian Shield: geochemical and isotopic evidence for a residual evaporite brine component. Geochim. Cosmochim. Acta 58 (5), 1483–1498.

Brand, E.L., 1986. Water and gas occurrences in the Evander Goldfield. In: Anhaeusser, C.R., Maske, S. (Eds.), Mineral Deposits of Southern Africa: Geological Society of South Africa, pp. 797–809.

Cano, R.J., Borucki, M.K., 1995. Revival and identification of bacterial spores in 25- to 40-million-year-old Dominican amber. Science 268 (5213), 1060–1064.

Chivian, D., Brodie, E.L., Alm, E.J., Culley, D.E., Dehal, P.S., DeSantis, T.Z., Gihring, T.M., Lapidus, A., Lin, L.-H., Lowry, S.R., Moser, D.P., Richardson, P.M., Southam, G., Wanger, G., Pratt, L.M., Andersen, G.L., Hazen, T.C., Brockman, F.J., Arkin, A.P., Onstott, T.C., 2008. Environmental genomics reveals a single-species ecosystem deep within Earth. Science 322 (5899), 275–278.

Craig, H., 1961. Isotopic variations in meteoric waters. Science 133 (3465), 1702–1703.

de Wit, M.J., de Ronde, C.E.J., Tredoux, M., Roering, C., Hart, R.J., Armstrong, R.A., Green, R.W.E., Peberdy, E., Hart, R.A., 1992. Formation of an Archaean continent. Nature 357 (6379), 553–562.

Drescher, J., Kirsten, T., Schäfer, K., 1998. The rare gas inventory of the continental crust, recovered by the KTB Continental Deep Drilling Project. Earth Planet. Sci. Lett. 154 (1–4), 247–263.

Frape, S.K., Fritz, P., 1987. Geochemical trends from groundwaters from the Canadian Shield. In: Fritz, P., Frape, S.K. (Eds.), Saline Waters and Gases in Crystalline Rocks: Geological Association of Canada, pp. 19–38.

Gihring, T.M., Moser, D.P., Lin, L.H., Davidson, M., Onstott, T.C., Morgan, L., Milleson, M., Kieft, T., Trimarco, E., Balkwill, D.L., Dollhopf, M., 2006. The distribution of microbial taxa in the subsurface water of the Kalahari Shield, South Africa. Geomicrobiol. J. 23, 415–430.

Grieve, R.A.F., Coderre, J.M., Robertson, P.B., Alexopoulos, J., 1990. Microscopic planar deformation features in quartz of the Vredefort structure: anomalous but still suggestive of an impact origin. Tectonophysics 171, 185–200.

Hünemohr, H., 1989. Edelgase in U- und Th-reichen Mineralen und die Bestimmung der 21Ne-Dicktargetausbeute der 18O(α, n)21Ne-Kernreaktion im Bereich 4.0–8.8 MeV, Ph.D. Thesis, Johannes-Gutenberg University Mainz, Mainz.

Johnson, M.R., Anhaeusser, C.R., Thomas, R.J. (Eds.), 2006. The Geology of South Africa: Geological Society of South Africa, Johannesburg/Council for Geosiences, Pretoria, p. 691.

Johnston, M.J.S., 2009. Near-field earthquake source mechanics at 3.6 depth, Tau Tona Mine, South Africa, IRIS Seismic Instrumentation Technology Symposium, Palm Springs, CA, USA.

Karl, D.M., Bird, D.F., Bjoerkman, K., Houlihan, T., Shackelford, R., Tupas, L., 1999. Microorganisms in the accreted ice of Lake Vostok, Antarctica. Science 286 (5447), 2144–2147.

Kennedy, B.M., Hiyagon, H., Reynolds, J.H., 1990. Crustal neon: a striking uniformity. Earth Planet. Sci. Lett. 98 (3–4), 277–286.

Kerr, R.A., 2002. Deep life in the slow, slow lane. Science 296 (5570), 1056–1058.

Klemd, R., 1999. A comparison of fluids causing post-depositional hydrothermal alteration in Archaean basement granitoids and the Witwatersrand Basin. Mineral. Petrol. 66 (1–3), 111–122.

Klemd, R., Hallbauer, D.K., Barton, J.M.J., 1989. Fluid inclusions studies of hydrothermally altered archaean granites around the Witwatersrand Basin. Mineral. Petrol. 40, 39–56.

Kloppmann, W., Girard, J.-P., Negrel, P., 2002. Exotic stable isotope compositions of saline waters and brines from the crystalline basement. Chem. Geol. 184 (1–2), 49–70.

Leroux, H., Reimold, W.U., Doukhan, J.C., 1994. A TEM investigation of shock metamorphism in quartz from the Vredefort Dome, South Africa. Tectonophysics 230, 223–239.

Lin, L.-H., Slater, G.F., Sherwood Lollar, B., Lacrampe-Couloume, G., Onstott, T.C., 2005a. The yield and isotopic composition of radiolytic H_2, a potential energy source for the deep subsurface biosphere. Geochim. Cosmochim. Acta 69 (4), 893–903.

Lin, L., Hall, J.A., Lippmann, J., Ward, J., Sherwood-Lollar, B., DeFlaun, M., Rothmel, R., Moser, D.P., Gihring, T.M., Mislowack, B., Onstott, T.C., 2005b. Radiolytic H_2 in continental crust: Nuclear power for deep subsurface microbial communities. Geochem. Geophys. Geosyst. 6, Q07003.

Lin, L.-H., Wang, P.-L., Rumble, D., Lippmann-Pipke, J., Boice, E., Pratt, L.M., Sherwood Lollar, B., Brodie, E.L., Hazen, T.C., Andersen, G.L., DeSantis, T.Z., Moser, D.P., Kershaw, D., Onstott, T.C., 2006. Long-term sustainability of a high-energy, low-diversity crustal biome. Science 314 (5798), 479–482.

Lippmann, J., Stute, M., Torgersen, T., Moser, D.P., Hall, J.A., Lin, L., Borcsik, M., Bellamy, R. E.S., Onstott, T.C., 2003. Dating ultra-deep mine waters with noble gases and ^{36}Cl, Witwatersrand Basin, South Africa. Geochim. Cosmochim. Acta 67 (23), 4597–4619.

Ma, L., Castro, M.C., Hall, C.M., 2009. Atmospheric noble gas signatures in deep Michigan Basin brines as indicators of a past thermal event. Earth Planet. Sci. Lett. 277 (1–2), 137–147.

Mason, B., Moore, C.B., 1981. Principles of Geochemistry. John Wiley, New York, N.Y. 344 pp.

Moser, D.P., Onstott, T.C., Fredrickson, J.K., Brockman, F.J., Balkwill, D.L., Drake, G.R., Pfiffner, S., White, D.C., Takai, K., Pratt, L.M., Fong, J., Sherwood-Lollar, B., Slater, G., Phelps, T.J., Spoelstra, N., DeFlaun, M., Southam, G., Welty, A.T., Baker, B.J., Hoek, J., 2003. Temporal shifts in microbial community structure and geochemistry of an ultradeep South African gold mine borehole. Geomicrobiol. J. 20, 1–32.

Niedermann, S., Bach, W., Erzinger, J., 1997. Noble gas evidence for a lower mantle component in MORBs from the southern East Pacific Rise: decoupling of helium and neon isotope systematics. Geochim. Cosmochim. Acta 61 (13), 2697–2715.

Niedermann, S., Schaefer, J.M., Wieler, R., Naumann, R., 2007. The production rate of cosmogenic ^{38}Ar from calcium in terrestrial pyroxene. Earth Planet. Sci. Lett. 257 (3–4), 596–608.

Nordstrom, D.K., Lindblom, S., Donahoe, R.J., Barton, C.C., 1989. Fluid inclusions in the Stripa granite and their possible influence on the groundwater chemistry. Geochim. Cosmochim. Acta 53 (8), 1741–1755.

Onstott, T.C., Lin, L.-H., Davidson, M., Mislowack, B., Borcsik, M., Hall, J., Slater, G.F., Ward, J.A., Sherwood Lollar, B., Lippmann-Pipke, J., Boice, E., Pratt, L.M., Pfiffner, S., Moser, D.P., Gihring, T.M., Kieft, T.L., Phelps, T.J., Heerden van, E., Litthaur, D., DeFlaun, M., Rothmel, R., Wanger, G., Southam, G., 2006. The origin and age of biogeochemical trends in deep fracture water of the Witwatersrand Basin, South Africa. Geomicrobiol. J. 23 (6), 369.

Parkes, R.J., Cragg, B.A., Bale, S.J., Getlifff, J.M., Goodman, K., Rochelle, P.A., Fry, J.C., Weightman, A.J., Harvey, S.M., 1994. Deep bacterial biosphere in Pacific Ocean sediments. Nature 371 (6496), 410–413.

Pedersen, K., 1997. Microbial life in deep granitic rock. Federation of European Microbiological Societies. Microbiol. Rev. 20 (2–3), 399–414.

Peeters, F., Beyerle, U., Aeschbach-Hertig, W., Holocher, J., Brennwald, M.S., Kipfer, R., 2002. Improving noble gas based paleoclimate reconstruction and groundwater dating using $^{20}Ne/^{22}Ne$ ratios. Geochim. Cosmochim. Acta 67 (4), 587–600.

Porcelli, D., Ballentine, C.J., Wieler, R., 2002. Noble gases in geochemistry and cosmochemistry. Rev. Mineral. Geochem. 47.

Priscu, J.C., Adams, E.E., Lyons, W.B., Voytek, M.A., Mogk, D.W., Brown, R.L., McKay, C.P., Takacs, C.D., Welch, K.A., Wolf, C.F., Kirshtein, J.D., Avci, R., 1999. Geomicrobiology of subglacial ice above Lake Vostok, Antarctica. Science 286 (5447), 2141–2144.

Robb, L.J., Meyer, F.M., 1995. The Witwatersrand Basin, South Africa: geological framework and mineralization processes. Ore Geol. Rev. 10, 67–94.

Robb, L.J., Charlesworth, E.G., Drennan, G.R., Gibson, R.L., Tongu, E.L., 1997. Tectono-metamorphic setting and paragenetic sequence of Au–U mineralisation in the Archaean Witwatersrand Basin, South Africa. Aust. J. Earth Sci. 44, 353–371.

Roedder, E., 1990. Fluid inclusions analysis — prologue and epilogue. Geochim. Cosmochim. Acta 54, 495–507.

Sherwood Lollar, B., Ballentine, C.J., 2009. Insights into deep carbon derived from noble gases. Progress Article. Nat. Geosci. 2, 543–547.

Sherwood Lollar, B., Frape, S.K., Weise, S.M., Fritz, P., Macko, S.A., Welhan, J.A., 1993. Abiogenic methanogenesis in crystalline rocks. Geochim. Cosmochim. Acta 57, 5087–5097.

Sherwood Lollar, B., Westgate, T.D., Ward, J.A., Slater, G.F., Lacrampe-Couloume, G., 2002. Abiogenic formation of alkanes in the Earth's crust as a minor source for global hydrocarbon reservoirs. Nature 416 (6880), 522–524.

Sherwood Lollar, B., Lacrampe-Couloume, G., Slater, G.F., Ward, J., Moser, D.P., Gihring, T.M., Lin, L.-H., Onstott, T.C., 2006. Unravelling abiogenic and biogenic sources of methane in the Earth's deep subsurface. Chem. Geol. 226 (3–4), 328–339.

Sherwood Lollar, B., Voglesonger, K., Lin, L.H., Lacrampe-Couloume, G., Telling, J., Abrajano, T.A., Onstott, T.C., Pratt, L.M., 2007. Hydrogeologic controls on episodic H_2 release from Precambrian fractured rocks: energy for deep subsurface life on Earth and Mars. Astrobiology 7 (6), 971–986.

Sherwood Lollar, B., Lacrampe-Couloume, G., Voglesonger, K., Onstott, T.C., Pratt, L.M., Slater, G.F., 2008. Isotopic signatures of CH_4 and higher hydrocarbon gases from Precambrian Shield sites: a model for abiogenic polymerization of hydrocarbons. Geochim. Cosmochim. Acta 72 (19), 4778–4795.

Sleep, N.H., Zoback, M.D., 2007. Did earthquakes keep the Early crust habitable? Astrobiology 7 (6), 1023–1032.

Stroncik, N.A., Niedermann, S., Haase, K.M., 2007. Neon and helium isotopes as tracers of mantle reservoirs and mantle dynamics. Earth Planet. Sci. Lett. 258 (1–2), 334–344.

Stuart, F.M., Turner, G., 1992. The abundance and isotopic composition of the noble gases in ancient fluids. Chem. Geol. 101 (1–2), 97–109.

Turner, G., Wang, S., Burgess, R., Bannon, M., 1988. Argon and other noble gases in fluid inclusions. Chem. Geol. 70 (1–2), 42.

Tweedie, E.B., 1986. The Evander goldfield. In: Anhaeusser, C.R., Maske, S. (Eds.), Mineral Deposits of Southern Africa: Geological Society of South Africa, pp. 705–730.

Vreeland, R.H., Rosenzweig, W.D., Powers, D.W., 2000. Isolation of a 250 million-year-old halotolerant bacterium from a primary salt crystal. Nature 407 (897–899).

Ward, J.A., Slater, G.F., Moser, D.P., Lin, L.-H., Lacrampe-Couloume, G., Bonin, A.S., Davidson, M., Hall, J.A., Mislowack, B., Bellamy, R.E.S., Onstott, T.C., Sherwood Lollar, B., 2004. Microbial hydrocarbon gases in the Witwatersrand Basin, South Africa: implications for the deep biosphere. Geochim. Cosmochim. Acta 68 (15), 3239–3250.

Wetherill, G.W., 1954. Variations in the isotopic abundances of neon and argon extracted from radioactive minerals. Phys. Rev. 96, 679–683.

Whiteside, H.C.M., Glasspool, K.R., Hiemstra, S.A., 1986. In: C. C.B. (Ed.), Gold in the Witwatersrand Triad: Min. Res. Rep. S. Afr. , pp. 39–73.

Whitman, W.B., Coleman, D.C., Wiebe, W.J., 1998. Prokaryotes: the unseen majority. Proc. Natl Acad. Sci. USA 95 (12), 6578–6583.

Zadnik, M.G., Jeffery, P.M., 1985. Radiogenic neon in an Archaean anorthosite. Chem. Geol. 52 (1), 119–125.